Rational Radial Distortion Models of Camera Lenses with Analytical Solution for Distortion Correction *

Lili Ma, YangQuan Chen† and Kevin L. Moore
Center for Self-Organizing and Intelligent Systems (CSOIS),
Dept. of Electrical and Computer Engineering, 4160 Old Main Hill,
Utah State University (USU), Logan, UT 84322-4160, USA.

Received (to be inserted by publisher)

The common approach to radial distortion is by the means of polynomial approximation, which introduces distortion-specific parameters into the camera model and requires estimation of these distortion parameters. The task of estimating radial distortion is to find a radial distortion model that allows easy undistortion as well as satisfactory accuracy. This paper presents a new class of rational radial distortion models with easy analytical undistortion formulae. Experimental results are presented to show that with this class of rational radial distortion models, satisfactory and comparable accuracy can be achieved.

Keywords: Camera calibration, radial distortion, radial undistortion, polynomial models, rational models.

1. Introduction

Cameras are widely used in many engineering automation processes from visual monitoring, visual metrology to real time visual servoing or visual following. We will focus on a new class of camera lens distortion models that are rational functions of simple polynomials and have analytical undistortion formulae, i.e., no numerical iteration is required for undistortion.

1.1. *Camera Calibration*

Camera calibration is to estimate a set of parameters that describes the camera's imaging process. With this set of parameters, a perspective projection matrix can directly link a point in the 3-D world reference frame to its projection (undistorted) on the image plane by:

$$\lambda \begin{bmatrix} u \\ v \\ 1 \end{bmatrix} = \mathbf{A}[\mathbf{R} \mid \mathbf{t}] \begin{bmatrix} X^w \\ Y^w \\ Z^w \\ 1 \end{bmatrix} = \begin{bmatrix} \alpha & \gamma & u_0 \\ 0 & \beta & v_0 \\ 0 & 0 & 1 \end{bmatrix} \begin{bmatrix} X^c \\ Y^c \\ Z^c \end{bmatrix}, \quad (1)$$

where (u, v) is the distortion-free image point on the image plane; the matrix $\mathbf{A}$ fully depends on the camera's five intrinsic parameters $(\alpha, \gamma, \beta, u_0, v_0)$ with (α, β) being two scalars in the two image axes, (u_0, v_0) the coordinates of the principal point, and γ describing the skewness of the two image axes; $[X^c, Y^c, Z^c]^T$ denotes a point in the camera frame which is related to the corresponding point $[X^w, Y^w, Z^w]^T$ in the world reference frame by $P^c = \mathbf{R}P^w + \mathbf{t}$ with $(\mathbf{R}, \mathbf{t})$ being the rotation matrix and the translation vector. For a variety of computer vision applications where camera is used as a sensor in

*Feb. 2004. Submitted to IJIA. Accepted 4/5/04.
†Corresponding author. Email: yqchen@ece.usu.edu. Tel: (435)7970148, Fax: (435)7973054, web: http://www.csois.usu.edu/

the system, the camera is always assumed fully calibrated beforehand.

The early works on precise camera calibration, starting in the photogrammetry community, use a 3-D calibration object whose geometry in the 3-D space is required to be known with a very good precision. However, since these approaches require an expensive calibration apparatus, camera calibration is prevented from being carried out broadly. Aiming at the general public, the camera calibration method proposed in [Zhang, 1999] focuses on desktop vision system and uses 2-D metric information. The key feature of the calibration method in [Zhang, 1999] is that it only requires the camera to observe a planar pattern at a few (at least three, if both the intrinsic and the extrinsic parameters are to be estimated uniquely) different orientations without knowing the motion of the camera or the calibration object. Due to the above flexibility, the calibration method in [Zhang, 1999] is used in this work, where the detailed procedures are summarized as: 1) estimation of intrinsic parameters, 2) estimation of extrinsic parameters, 3) estimation of distortion coefficients, and 4) nonlinear optimization. The overall calibration procedures are illustrated in Fig. 1.

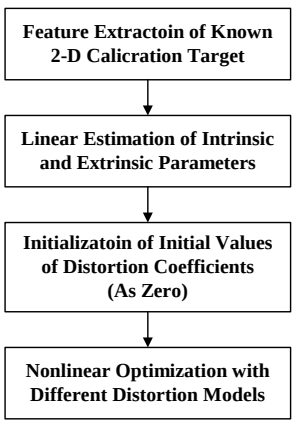

Fig. 1. Camera calibration procedures.

1.2. *Radial Distortion*

In equation (1), (u, v) is not the actually observed image point since virtually all imaging devices introduce certain amount of nonlinear distortions. Among the nonlinear distortions, radial distortion, which is performed along the radial direction from the center of distortion, is the most severe part [Devernay and Faugeras, 2001; Tsai, 1987]. The radial distortion causes an inward or outward displacement of a given image point from its ideal location. The negative radial displacement of the image points is referred to as the barrel distortion, while the positive radial displacement is referred to as the pincushion distortion [Weng et al., 1992]. The removal or alleviation of the radial distortion is commonly performed by first applying a parametric radial distortion model, estimating the distortion coefficients, and then correcting the distortion.

Lens distortion is very important for accurate 3-D measurement [Lenz and Tsai, 1988]. Let (u_d, v_d) be the actually observed image point and assume that the center of distortion is at the principal point. The relationship between the undistorted and the distorted radial distances is given by

$$r_d = r + \delta_r, \tag{2}$$

where r_d is the distorted radial distance and δ_r the radial distortion (some other variables used throughout this paper are listed in Table 1).

Table 1. List of Variables

Variable	Description
$(u_d,\, v_d)$	Distorted image point in pixel
$(u,\, v)$	Distortion-free image point in pixel
$(x_d,\, y_d)$	$[x_d,\, y_d,\, 1]^T = \mathbf{A}^{-1}[u_d,\, v_d,\, 1]^T$
$(x,\, y)$	$[x,\, y,\, 1]^T = \mathbf{A}^{-1}[u,\, v,\, 1]^T$
r_d	$r_d^2 = x_d^2 + y_d^2$
r	$r^2 = x^2 + y^2$
$\mathbf{k}$	Radial distortion coefficients

Most of the existing works on the radial distortion models can be traced back to an early study in photogrammetry [Slama, 1980] where the radial distortion is governed by the following polynomial equation [Zhang, 1999; Slama, 1980; Heikkil and Silvn, 1997; Heikkila and Silven, 1996]:

$$r_d = r\, f(r) = r\,(1 + k_1 r^2 + k_2 r^4 + k_3 r^6 + \cdots), \tag{3}$$

where $k_1, k_2, k_3, \ldots$ are the distortion coefficients. It follows that

$$x_d = x\, f(r), \quad y_d = y\, f(r), \tag{4}$$

which is equivalent to

$$u_d - u_0 = (u - u_0) f(r), v_d - v_0 = (v - v_0) f(r). \quad (5)$$

For the polynomial radial distortion model (3) and its variations, the distortion is especially dominated by the first term and it has also been found that too high an order may cause numerical instability [Zhang, 1999; Tsai, 1987; Wei and Ma, 1994]. When using two coefficients, the relationship between the distorted and the undistorted radial distances becomes [Zhang, 1999]

$$r_d = r\,(1 + k_1\,r^2 + k_2\,r^4). \quad (6)$$

The inverse of the polynomial function (6) is difficult to perform analytically, but can be obtained numerically via an iterative scheme.

Besides the commonly used radial distortion modeling (3), the relationship between r_d and r can also be modelled as [Hartley and Zisserman, 2000]

$$r_d = r\,f(r) = r\,(1 + k_1 r + k_2 r^2 + k_3 r^3 + \ldots). \quad (7)$$

To overcome the inversion problem, the above model with two coefficients is studied in [Ma et al., 2003], which is

$$f(r) = 1 + k_1\,r + k_2\,r^2, \quad (8)$$

whose appealing feature lies in its satisfactory accuracy as well as the existence of an easy analytical undistortion formula.

Until recently, the most commonly used radial distortion models are still in the polynomial form, though other models, such as the division model [Fitzgibbon, 2001] and the fish-eye radial distortion models (the Fish Eye Transform [Devernay and Faugeras, 2001] and the Field-Of-View [Basu and Licardie, 1995]), are available in the literature. A rational model in the form of

$$r_d = \frac{\sqrt{1 + 4kr^2} - 1}{2kr} \quad (9)$$

is proposed in [Brauer-Burchardt and Voss, 2001] when r_d and r are expressed in the camera frame. However, it is not specified clearly in [Brauer-Burchardt and Voss, 2001] why this model is sought.

In this work, a new class of rational radial distortion models that are functions of simple polynomials is proposed. In the full-scale nonlinear optimization, the following objective function [Zhang, 1999]:

$$J = \sum_{i=1}^{N} \sum_{j=1}^{n} \|m_{ij} - \hat{m}(\mathbf{A}, \mathbf{k}, \mathbf{R}_i, \mathbf{t}_i, M_j)\|^2, \quad (10)$$

is used, where M_j is the j^{th} 3-D point in the world frame with $Z^w = 0$; $\hat{m}(\mathbf{A}, \mathbf{k}, \mathbf{R}_i, \mathbf{t}_i, M_j)$ is the projection of point M_j in the i^{th} image using the estimated parameters; $\mathbf{k}$ denotes the distortion coefficients; n is the number of feature points in the coplanar calibration object; and N[a] is the number of images taken for calibration. In [Zhang, 1999], the estimation of radial distortion is done after having estimated the intrinsic and the extrinsic parameters and just before the nonlinear optimization step. So, for different radial distortion models, we can reuse the estimated intrinsic and extrinsic parameters. The quantities M_j is known during the calibration process. Knowledge of M_j comes from the known calibration target, which is a 2-D planar surface in our study. The quantities $\mathbf{R}_i$ and $\mathbf{t}_i$ are not fixed during nonlinear optimizations.

The rest of the paper is organized as follows. Section 2 briefly describes the analytical distortion model (8) and its radial undistortion. The new class of rational radial distortion models is presented in Sec. 3. The proposed rational radial distortion functions are extensively validated in Sec. 4 by performing a series of simulations and experiments using both real manufactured cameras and a simulated virtual camera, where issues such as model selection and evaluation of only the distortion are addressed in detail. Finally, some discussions and concluding remarks are given in sections 5 and 6, respectively.

2. Analytical Polynomial Radial Distortion Model

2.1. *Model*

The conventional radial distortion model (6) does not have an exact inverse. Existing meth-

[a] n and N are chosen to be $n = 256$ and $N = 5$ in the experiments performed in this paper.

ods to overcome the problem of no analytical inverse function include:

(a) Via iterative numerical method.
(b) Preparing a table containing the inverse relationship and searching through the table for the inverse.
(c) Using approximations, such as [Heikkila, 2000]

$$r_d = r(1+k_1 r^2+k_2 r^4) \leftrightarrow r = r_d(1-k_1 r_d^2-k_2 r_d^4) \quad (11)$$

and [Fitzgibbon, 2001]

$$r_d = r(1+k_1 r^2) \leftrightarrow r = \frac{r_d}{1+k_1 r_d^2}. \quad (12)$$

The fitting results given by the above approximations can be satisfactory when the distortion coefficients are small values. However, an extra source of error is introduced and this will inevitably degrade the calibration accuracy.

The above listed three methods introduce either additional computation time or additional approximation errors. Due to these reasons, an analytical inverse function that has the advantage of giving the exact undistortion solution is one of the main focus of this work. To overcome the shortcoming of no analytical inverse formula but still preserving a comparable accuracy, the radial distortion model (8) that has the following three properties has been studied in [Ma et al., 2003]:

(a) This function is radially symmetric around the center of distortion (which is assumed to be at the principal point (u_0, v_0) for our discussion) and it is expressible in terms of radius r only.
(b) This function is continuous and derivable, hence $r_d = 0$ iff $r = 0$ within the reasonable range of r.
(c) The resultant approximation of x_d is an odd function of x. For example, from (8), we have

$$\begin{cases} x_d = x\, f(r) = x\,(1+k_1 r+k_2 r^2) \\ y_d = y\, f(r) = y\,(1+k_1 r+k_2 r^2) \end{cases}. \quad (13)$$

It is obvious that $x_d = 0$ iff $x = 0$. When $x_d \neq 0$, by letting $\kappa = y_d/x_d = y/x$, we have $y = \kappa x$ where κ is a constant. Substituting $y = \kappa x$ into the above equation gives:

$$\begin{aligned} x_d &= x\left[1+k_1\sqrt{x^2+\kappa^2 x^2}+k_2(x^2+\kappa^2 x^2)\right] \\ &= x + k_1\sqrt{1+\kappa^2}\,\mathtt{sgn}(x)\,x^2 + k_2(1+\kappa^2)\,x^3, \end{aligned}$$

where $\mathtt{sgn}(x)$ gives the sign of x and x_d is an odd function of x. Thus, when interpreting from the relationship between (x_d, y_d) and (x, y) in the camera frame, the radial distortion function is to approximate the $x_d \leftrightarrow x$ relationship which is intuitively an odd function.

Remark 2.1 *The radial distortion models discussed in this paper belong to the category of Undistorted-Distorted model, while the Distorted-Undistorted model also exists in the literature to correct the distortion [Tamaki et al., 2002]. The radial distortion models can be applied to the D-U formulation simply by defining*

$$r = r_d\, f(r_d).$$

Consistent results and improvement can be achieved in the above D-U formulation. While a D-U formulation relieves us the task of performing undistortion, in some cases, it is still desirable to locate the projection of a 3-D point on the image plane knowing its 3-D coordinates.

2.2. *Analytical Radial Undistortion*

From equations (7) and (8),

$$k_2 r^3 + k_1 r^2 + r - r_d = 0. \quad (14)$$

By letting $a = k_1/k_2, b = 1/k_2$, and $c = -r_d/k_2$, we have

$$r^3 + a\,r^2 + b\,r + c = 0. \quad (15)$$

Further, let $\bar{r} = r + a/3$. The above equation becomes $\bar{r}^3 + p\,\bar{r} + q = 0$, where $p = b - a^2/3$ and $q = 2a^3/27 - ab/3 + c$. Let $\Delta = (\frac{q}{2})^2 + (\frac{p}{3})^3$. If $\Delta > 0$, there is only one solution; if $\Delta = 0$, then $r = 0$, which occurs when $\delta_r = 0$; if $\Delta < 0$, then there are three solutions [Pearson, 1983]. In general, the middle one is what we need, since the first root is at a negative radius and the third lies beyond the positive turning point [Zhang, 1996; Tordoff, 2002]. After r is determined, (u, v) can be calculated from (5) directly.

3. Rational Radial Distortion Models

3.1. *Rational Models*

Based on the three criteria listed in Sec. 2.1, a new class of radial distortion models (models #5, 6, 7, 8, 9, 10) are proposed and summarized in Table 2, where the other four polynomial models (models #1, 2, 3, 4) are also listed. Using these models, the $x_d \leftrightarrow x$ relationship complies with the property of being an odd function, as shown in the third column in Table 2.

Clearly, all these functions in Table 2, except the function #4, are special cases of the following function

$$f(r, \kappa) = \frac{1 + \kappa_1 r + \kappa_2 r^2}{1 + \kappa_3 r + \kappa_4 r^2 + \kappa_5 r^3}. \quad (16)$$

The function #4 in Table 2 is the most commonly used radial distortion function in the polynomial approximation category. The other nine functions in Table 2 are studied specifically with the goal to achieve comparable performance with the function #4 using the least amount of model complexity and as few distortion coefficients as possible. Since the functions #9, 10 in Table 2 begin to show comparable calibration performance to the function #4 (as can be seen later in Sec. 4), more complex distortion functions are not studied in this work.

3.2. *Radial Undistortion of the Rational Models*

The rational functions listed in Table 2 are all special cases of the function (16). Radial undistortion of the proposed rational functions are illustrated in the next using the general function (16). From (16), we have

$$r_d = r f(r) = r \frac{1 + \kappa_1 r + \kappa_2 r^2}{1 + \kappa_3 r + \kappa_4 r^2 + \kappa_5 r^3}. \quad (17)$$

After simple mathematical derivations,

$$(r_d k_5 - k_2) r^3 + (r_d k_4 - k_1) r^2 + (r_d k_3 - 1) r + r_d = 0. \quad (18)$$

By letting

$$a = \frac{r_d k_4 - k_1}{r_d k_5 - k_2},\ b = \frac{r_d k_3 - 1}{r_d k_5 - k_2},\ c = \frac{r_d}{r_d k_5 - k_2},$$

we arrive at equation (15). Following the procedures described in Sec. 2.2, radial undistortion of the general rational function (16) can be performed analytically with a closed-form solution.

4. Experimental Results

A series of experiments are performed in this section to validate the proposed rational distortion models. First, the final values of the objective function J defined in (10) of three groups of testing images are given in Sec. 4.1. The model selection problem among the ten models in Table 2 is further discussed using the geometric AIC (Akaike Information Criterion) and the geometric MDL (Minimum Description Length) criteria [Kanatani, 2002; El-Melegy and Farag, 2003] in Sec. 4.2. Then, we simulate the whole imaging process by constructing a virtual camera with known camera parameters and radial distortion in Sec. 4.3. We generate images with noise of a planar calibration target. At a second time, we test if the distortion coefficients are accurately estimated by observing the resultant $f(r) \leftrightarrow r$ curves.

4.1. *Initial Model Comparison*

For the proposed rational distortion functions (models #5, 6, 7, 8, 9, 10), comparisons are first made with the other four polynomial functions (models #1, 2, 3, 4) based on the final values of the objective function J in (10) after nonlinear optimization by the Matlab function `fminunc`, since common approach to the camera calibration is to perform a full-scale nonlinear optimization for all parameters. Using the public domain testing images (640×480 in pixel) [Zhang, 1998], the desktop camera images (320×240) [Ma et al., 2002] (a color camera in our CSOIS), and the ODIS camera images (320×240) [Ma et al., 2002] (the camera on ODIS robot built in our CSOIS), the final values of J, the estimated distortion coefficients, and the five estimated intrinsic parameters $(\alpha, \beta, \gamma, u_0, v_0)$, are shown in Tables 3, 4, and 5, respectively. The extracted corners for the model plane of the desktop and the ODIS cameras are shown in Figs. 2 and 3. As noticed from these images, the two cameras

Table 2. Distortion Models

#	$f(r)^*$	$x_d = f(x)$
1	$1 + k\,r$	$x \cdot (1 + k\sqrt{1+c^2}\,x\,sgn(x))$
2	$1 + k\,r^2$	$x \cdot (1 + k\,(1+c^2)\,x^2)$
3	$1 + k_1\,r + k_2\,r^2$	$x \cdot (1 + k_1\,\sqrt{1+c^2}\,x\,sgn(x) + k_2\,(1+c^2)\,x^2)$
4	$1 + k_1\,r^2 + k_2\,r^4$	$x \cdot (1 + k_1\,(1+c^2)\,x^2 + k_2\,(1+c^2)^2\,x^4)$
5	$\frac{1}{1 + k\,r}$	$x \cdot \frac{1}{1 + k\,\sqrt{1+c^2}\,x\,sgn(x)}$
6	$\frac{1}{1 + k\,r^2}$	$x \cdot \frac{1}{1 + k\,(1+c^2)\,x^2}$
7	$\frac{1 + k_1\,r}{1 + k_2\,r^2}$	$x \cdot \frac{1 + k_1\,\sqrt{1+c^2}\,x\,sgn(x)}{1 + k_2\,(1+c^2)\,x^2}$
8	$\frac{1}{1 + k_1\,r + k_2\,r^2}$	$x \cdot \frac{1}{1 + k_1\sqrt{1+c^2}\,x\,sgn(x) + k_2\,(1+c^2)\,x^2}$
9	$\frac{1 + k_1\,r}{1 + k_2\,r + k_3\,r^2}$	$x \cdot \frac{1 + k_1\sqrt{1+c^2}\,x\,sgn(x)}{1 + k_2\,\sqrt{1+c^2}\,x\,sgn(x) + k_3\,(1+c^2)\,x^2}$
10	$\frac{1 + k_1\,r^2}{1 + k_2\,r + k_3\,r^2}$	$x \cdot \frac{1 + k_1\,(1+c^2)\,x^2}{1 + k_2\,\sqrt{1+c^2}\,x\,sgn(x) + k_3\,(1+c^2)\,x^2}$

*With the risk of introducing some confusion, the same symbols k_1, k_2, and k_3 are used in different models that might have different values.

both experience a barrel distortion[b]. In the experiments, we use a planar calibration target that contains 256 feature points. Five images are taken for each calibration.

Tables 3, 4, and 5 are of the same format. The first column is the model number consistent with what in Table 2. The second column shows the values of objective function J defined in (10). The third column, the rank, sorts the distortion models by J in a [1-smallest, 10-largest] manner. From Tables 3, 4, and 5, we have the following observations:

(a) Using the proposed rational models, comparable, or even better, results can be achieved compared with the polynomial model #4 in Table 2, at the cost of introducing an extra distortion coefficient.
(b) For each category of models, either polynomial or rational, they generally follow the trend that the more complex the model, the smaller the fitting residual J.
(c) When the distortion is significant, the performance improvement using complex models becomes more obvious.

The comparison based on J in Tables 3, 4, and 5 might not be fair since the distortion models use different numbers of distortion coefficients. Due to this concern, more simulations and discussions are presented in sections 4.2 and 4.3 for the validation of the proposed rational models regarding their accuracy improvement and stability. Our main point is to emphasize that, by applying the rational functions, comparable accuracy can be achieved without sacrificing the property of having analytical undistortion function.

To make the results in this paper repeatable by other researchers for further investigation, we present the options we use for the nonlinear optimization: `options = optimset('Display', 'iter', 'LargeScale', 'off', 'MaxFunEvals', 8000, 'TolX', 10^-5, 'TolFun', 10^-5, 'MaxIter', 120)`.

[b]The plotted dots in the center of each square are only used for judging the correspondence with the world reference points.

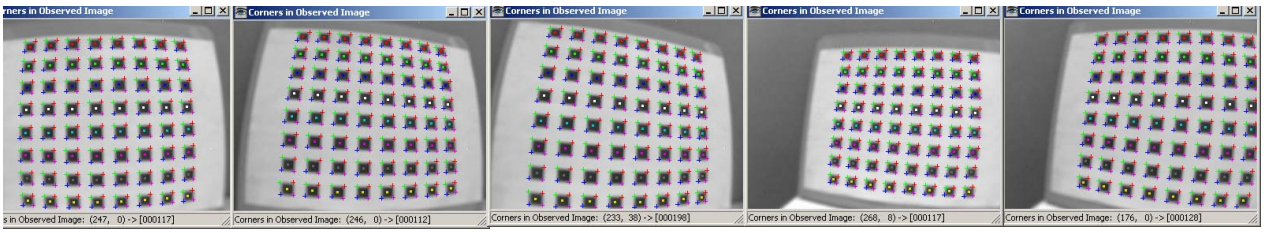

Fig. 2. Five images of the model plane with the extracted corners (indicated by cross) for the desktop camera.

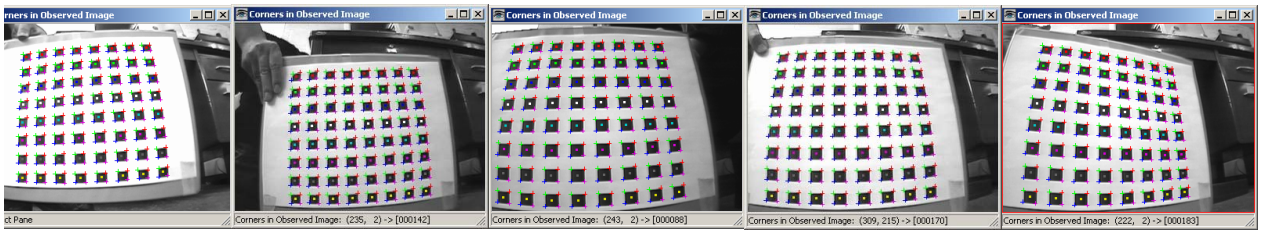

Fig. 3. Five images of the model plane with the extracted corners (indicated by cross) for the ODIS camera.

Table 3. Comparison Results using Microsoft Images

#	J	Rank	Final Values of k			Final Values of $(\alpha, \gamma, u_0, \beta, v_0)$				
1	180.5714	9	-0.0984	-	-	845.305	0.191	303.572	845.262	208.439
2	148.2789	8	-0.1984	-	-	830.742	0.216	303.948	830.798	206.557
3	145.6592	6	-0.0215	-0.1566	-	833.650	0.207	303.984	833.686	206.555
4	144.8802	**3**	-0.2286	0.1905	-	832.486	0.204	303.960	832.515	206.581
5	185.0628	10	0.1031	-	-	846.130	0.192	303.507	846.082	208.694
6	147.0000	7	0.2050	-	-	831.086	0.213	303.964	831.136	206.517
7	145.4682	5	-0.0174	0.1702	-	833.397	0.207	303.968	833.432	206.556
8	145.4504	**4**	0.0170	0.1725	-	833.384	0.206	303.971	833.419	206.544
9	144.8328	**2**	1.6457	1.6115	0.4054	830.941	0.204	303.957	830.970	206.583
10	144.8257	**1**	1.2790	-0.0119	1.5478	831.737	0.204	303.957	831.766	206.592

4.2. *Distortion Model Selection*

Classical criteria that are used in the computer vision to assess the accuracy of calibration includes the radial distortion as one part inherently [Weng et al., 1992]. However, the idea to chose among candidate models the one that gives the smallest residual does not work, because a model with more degrees of freedom might always be chosen since it is more likely to yield a smaller residual. To compare the distortion models fairly, the over-fit caused by more degrees of freedom in the distortion model needs to be compensated. Due to the above concern, a comparison that is solely based on the fitting residual of the full-scale nonlinear optimization, as performed in Sec. 4.1, is not enough.

Model selection is one of the central subjects of statistical inference. In [Kanatani, 2002], two widely adopted criteria for statistical model selection, Akaike's AIC and Rissanen's MDL, have been generalized to be GAIC and GMDL for the geometric fitting such that the generalized GAIC and GMDL can be helpful for geometric problems considered in the computer vision. The GAIC and GMDL of a model S are defined as

Table 4. Comparison Results using Desktop Images

#	**J** ($\times 10^3$)	**Rank**	**Final Values of** k			**Final Values of** $(\alpha, \gamma, u_0, \beta, v_0)$				
1	1.0167	9	-0.2466	-	-	295.573	-0.819	156.610	288.876	119.852
2	0.9047	8	-0.2765	-	-	275.595	-0.666	158.201	269.230	121.525
3	0.8033	7	-0.1067	-0.1577	-	282.564	-0.619	154.491	275.901	120.092
4	0.7790	**1**	-0.3435	0.1232	-	277.144	-0.573	153.988	270.558	119.810
5	1.2018	10	0.3045	-	-	302.233	-1.023	160.560	295.676	120.744
6	0.7986	6	0.3252	-	-	276.252	-0.578	154.797	269.706	120.323
7	0.7876	5	-0.0485	0.2644	-	279.506	-0.588	154.173	272.882	119.956
8	0.7864	**4**	0.0424	0.2834	-	279.326	-0.587	154.116	272.704	119.921
9	0.7809	**3**	0.5868	0.5271	0.5302	275.831	-0.573	153.999	269.282	119.819
10	0.7800	**2**	0.2768	-0.0252	0.6778	276.450	-0.573	153.991	269.885	119.809

Table 5. Comparison Results using ODIS Images

#	**J** ($\times 10^3$)	**Rank**	**Final Values of** k			**Final Values of** $(\alpha, \gamma, u_0, \beta, v_0)$				
1	0.9444	9	-0.2327	-	-	274.266	-0.115	140.362	268.307	114.391
2	0.9331	8	-0.2752	-	-	258.319	-0.516	137.215	252.685	115.930
3	0.8513	6	-0.1192	-0.1365	-	266.085	-0.367	139.919	260.313	113.241
4	0.8403	**3**	-0.3554	0.1633	-	260.765	-0.274	140.058	255.148	113.172
5	1.0366	10	0.2828	-	-	278.021	-0.028	139.594	271.927	116.299
6	0.8676	7	0.3190	-	-	259.494	-0.430	139.125	253.869	113.961
7	0.8450	5	-0.0815	0.2119	-	264.403	-0.350	140.052	258.680	113.144
8	0.8438	**4**	0.0725	0.2419	-	264.134	-0.342	140.109	258.420	113.112
9	0.8379	**1**	1.2859	1.1839	0.7187	259.288	-0.282	140.293	253.704	113.007
10	0.8383	**2**	0.4494	-0.0124	0.8540	260.937	-0.280	140.243	255.317	113.056

[Kanatani, 2002; El-Melegy and Farag, 2003]:

$$\text{GAIC}(S) = J(S) + 2(dD + p)\varepsilon^2, \qquad (19)$$

and

$$\text{GMDL}(S) = J(S) - (dD + p)\varepsilon^2 \log(\varepsilon/L)^2, \qquad (20)$$

where $J(S)$ is the fitting residual when data of size D are fitted to the model S. p is the degree of freedom (DOF) of the model S. $d = m - r$ with m the dimension of the observed data and r the co-dimension of the model. L is a reference length, which is taken to be the image width in [El-Melegy and Farag, 2003]. ε is the noise level in the data set.

In the context of lens distortion modeling, in order to apply the GAIC and GMDL, the noise level ε needs to be known. An unbiased estimate of ε can be obtained from the most commonly used candidate model (6), denoted by S^0, as [Kanatani, 2002; El-Melegy and Farag, 2003]:

$$\hat{\varepsilon}^2 = \frac{J(S^0)}{rD - p^0}, \qquad (21)$$

where p^0 is the DOF of the model S^0.

Naturally, interests arose about using the MDL criterion, since it is regarded by many as superior to the AIC criterion for statistical inference. It was thus anticipated that a criterion like MDL would outperform the geometric AIC for geometric fitting, too [Kanatani, 2002]. However, it has been reported in [Kanatani, 2002] that the above anticipation is negative. In this experiment, both the GAIC and GMDL are applied to validate the proposed model relevance, where the results are shown in Table 6. The first column "#" denotes the model number consistent with what in Table 2. The quantities under "GAIC" and "GMDL" are the calculated values

using (19) and (20), respectively, where an unbiased estimate of ε is obtained from the most commonly used candidate model (6). To calculate the GMDL, the reference length L is chosen to the width of the image [El-Melegy and Farag, 2003]. That is, L is chosen to be 640, 320, and 320 for the public, the desktop, and the ODIS images. To facilitate an easy comparison, the rank that sorts the ten models by the GAIC and GMDL criteria in a [1-smallest, 10-largest] manner are provided as subscripts associated with each quantity.

Table 6 deserves a careful observation. For the three groups of testing images, the GAIC criterion generally favors the models $\#4, 7, 8, 9, 10$ (though not necessarily in the same order), more than the other five models. When using the GMDL criterion, other than selecting models $\#7, 8, 9, 10$ for the desktop and the ODIS camera, for the public image, it favors the models #3 and 6. In fact, this phenomenon is not surprising, since when the distortion is not significant, it is natural that the advantage gained by using more complex models can not be paid off. Further, the penalty for one degree of freedom is heavier in the GMDL than in the GAIC (see (19) and (20)). Thus, the GAIC is more faithful to the data than the GMDL, which is more likely to choose a degenerate model [Kanatani, 2002]. In summary, the proposed rational functions, at least the functions $\#7, 8, 9, 10$, provide comparable alternatives to the commonly used model #4 concerning the calibration accuracy and the property of having analytical inverse formulae. Notice that, in the comparison performed in Table 6, the model #4 is treated as the ground truth model.

4.3. *Evaluation of Distortion Only*

The GAIC and GMDL based model selection, as presented in Sec. 4.2, uses the fitting residual after the nonlinear optimization process with the extra DOF in the distortion model being compensated. In this section, we want to imagine the measurements that involves the distortion only. This is based on the idea that if the distortion coefficients are accurately estimated, the resultant $f(r) \leftrightarrow r$ curves should be close to the true curve. Since the true values of the intrinsic parameters and the distortion coefficients are by no means exactly known from a manufactured camera as used in sections 4.1 and 4.2, we construct a virtual camera via simulation to evaluate the distortion calibration. Besides, we also consider how the initial values of the intrinsic and extrinsic parameters affect the final selection of the distortion model.

When constructing the virtual camera, we assume that the camera has the following parameters:

(a) Intrinsic matrix:

$$\mathbf{A} = \begin{bmatrix} 260 & -0.2741 & 140.0581 \\ 0 & 255.1489 & 113.1727 \\ 0 & 0 & 1 \end{bmatrix}. \qquad (22)$$

(b) Distortion model: $f(r) = 1 - 0.3554r^2 + 0.1633r^4$.

(c) Extrinsic matrix: $\mathbf{RT} =$

$$\begin{bmatrix} -1.89 & 2.83 & -1.95 & 12.16 & -12.64 & -31.90 \\ -1.26 & 2.94 & -1.29 & 10.39 & -16.31 & -33.44 \\ -1.51 & 2.78 & -1.53 & 13.03 & -12.09 & -24.50 \\ -1.46 & 2.81 & -1.47 & 12.88 & -13.07 & -27.26 \\ -0.80 & 2.59 & -0.74 & 11.16 & -11.69 & -23.99 \end{bmatrix}, \qquad (23)$$

where each row in (23) denotes the transformation between the camera and the world coordinate system, and where the first three elements in each row in $\mathbf{RT}$ denote the ZYZ Euler angles $(\theta_a, \theta_b, \theta_c)$ such that the rotation matrix $\mathbf{R}$ can be calculated by:

$$\mathbf{R} = \mathbf{R}_z(\theta_a)\,\mathbf{R}_y(\theta_b)\,\mathbf{R}_z(\theta_c), \qquad (24)$$

with

$$\mathbf{R}_z(\theta_c) = \begin{bmatrix} \cos(\theta_c) & -\sin(\theta_c) & 0 \\ \sin(\theta_c) & \cos(\theta_c) & 0 \\ 0 & 0 & 1 \end{bmatrix}, \quad \mathbf{R}_y(\theta_b) = \begin{bmatrix} \cos(\theta_b) & 0 & \sin(\theta_b) \\ 0 & 1 & 0 \\ -\sin(\theta_b) & 0 & \cos(\theta_b) \end{bmatrix}. \qquad (25)$$

The remaining three elements denote the translational vector. The matrix $\mathbf{RT}$ has five rows to simulate the usage of five images for the camera calibration. The distortion model selected in the form of (6) is due to its common usage and acceptance. The simulated camera is close to the ODIS camera shown in Table 5.

Table 6. Model Selection Using the GAIC and GMDL Criteria

	#	**Public** ($L = 640$)		**Desktop** ($L = 320$)		**ODIS** ($L = 320$)	
		GAIC	GMDL(10^3)	GAIC(10^3)	GMDL(10^4)	GAIC(10^3)	GMDL(10^4)
Polynomial	1	471.0120_{9}	2.3734_{9}	2.5784_{9}	1.0411_{9}	2.6289_{9}	1.1014_{9}
	2	438.7195_{8}	2.3411_{8}	2.4663_{8}	1.0299_{8}	2.6176_{8}	1.1003_{8}
	3	436.3266_{6}	2.3402_{5}	2.3661_{7}	1.0205_{7}	2.5371_{6}	1.0929_{6}
	4	435.5476_{1}	2.3394_{1}	2.3418_{1}	1.0181_{1}	2.5261_{3}	1.0918_{1}
Rational	5	475.5034_{10}	2.3779_{10}	2.7634_{10}	1.0596_{10}	2.7211_{10}	1.1106_{10}
	6	437.4406_{7}	2.3398_{2}	2.3602_{6}	1.0193_{6}	2.5521_{7}	1.0937_{7}
	7	436.1356_{5}	2.3400_{4}	2.3504_{5}	1.0189_{4}	2.5308_{5}	1.0923_{3}
	8	436.1178_{4}	2.3400_{3}	2.3492_{4}	1.0188_{2}	2.5296_{4}	1.0921_{2}
	9	435.7269_{3}	2.3411_{7}	2.3450_{3}	1.0190_{5}	2.5250_{1}	1.0923_{4}
	10	435.7198_{2}	2.3411_{6}	2.3441_{2}	1.0189_{3}	2.5254_{2}	1.0924_{5}

First, consider the influence of different initial values for the final distortion model selection. While different methods using the same data set might obtain different initial values, what we simulate here sticks to the same method to obtain the initial values but with corrupted simulated images. The simulated calibration process is performed when noise levels of 0, 0.25, 0.5, and 0.75[c] are applied to the ideal simulated (u_d, v_d) that is calculated using the assumed camera parameters in (22) and (23). For each noise level, five sets of corrupted images are generated, where each set contains five images for the calibration. We average the five sets of calibration results and use the average for comparison.

Since we are mainly interested in how the initial values influence the final selection of the distortion model, detailed values of $J, (\alpha, \gamma, u_0, \beta, v_0)$, and $\mathbf{k}$ are not given. Only the model numbers in a sorted manner are presented in Table 7, under the above four different noise levels using the GAIC and the GMDL criteria, where the GMDL quantities are written in an Italian format.

Quantities in Table 7 manifests a similar trend as already shown in Table 6, in the sense that the GAIC criterion shows a consistent selection of the rational models $\#7, 8, 9, 10$ among the top five models (not necessarily in the same order). However, when using the GMDL criterion, as the noise level increases, that is, as the initial values deviate from their "true values", the GMDL criterion chooses models $\#3, 6$ over $\#9, 10$ to be among the top five. Again, this is due to the tendency in the GMDL to select a degenerate model of less coefficients, model #6 (one coefficient) over #4 (two coefficients) and model #3 (two coefficients) over models $\#9, 10$ (three coefficients).

Table 7. Model Selection of the Simulated Camera

Noise Level	**Model #** ⟵ Better … Worse ⟶									
0	4	10	9	8	7	6	3	2	1	5
	4	*10*	*9*	*8*	*7*	*6*	*3*	*2*	*1*	*5*
0.25	4	10	9	8	7	3	6	2	1	5
	4	*8*	*7*	*10*	*9*	*6*	*3*	*2*	*1*	*5*
0.50	4	10	9	8	7	3	6	2	1	5
	6	*4*	*8*	*7*	*3*	*10*	*9*	*2*	*1*	*5*
0.75	4	8	7	9	10	3	6	2	1	5
	6	*4*	*8*	*7*	*3*	*10*	*9*	*2*	*1*	*5*

*The rows written in the Italian format are the GMDL values. Others are the GAIC values.

It is interesting to see from Table 7 that as the noise level increases, the GMDL criterion would not even choose the model #4, though this is the assumed "true" model with noise corruption. A possible explanation of this phe-

[c]The noise is generated using the Matlab command `randn(·)` multiplied with the corresponding noise level.

nomenon is that, when the feature extraction could not guarantee certain precision, the camera parameters can not be estimated accurately.

The resultant $f(r) \leftrightarrow r$ curves are illustrated in Fig. 4 under noise level 0.25 (Fig 4 a) and 0.75 (Fig 4 b), respectively. In each figure, the $f(r) \leftrightarrow r$ curves of models $\#3, 4, 6, 7, 8, 9, 10$ are plotted. It can be observed that the plotted curves are very close to each other and also to the true curve. In Fig. 4, each curve is not specifically labelled since the main purpose here is to demonstrate the stability property of using different distortion models, rather than selecting one specific model qualitatively from these $f(r) \leftrightarrow r$ curves.

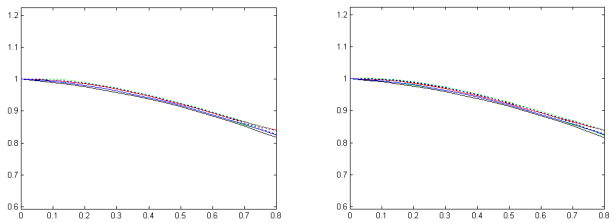

Fig. 4. $f(r) \leftrightarrow r$ curves for the simulated camera using the models $\#3, 4, 6, 7, 8, 9, 10$ in Table 2.

Till this point, it is safe to claim that the proposed class of rational functions provide an alternative for the commonly used rational distortion model (6), as far as both the calibration accuracy and the optimization stability are concerned. It is also worthy mentioning that whether a certain distortion model best represents a lens distortion is indeed camera-dependent. Thus, it is not surprising that for some cameras, the proposed rational functions might out outperform their polynomial counterparts.

5. Discussions

This section presents some discussions regarding the advantage of the proposed rational radial distortion models and how to extend them to include tangential distortion.

(a) **Why new rational models?** The traditional model (6) has been widely used in the radial distortion modelling due to its accuracy and its physical basis. Though it is also widely admitted that this model has no analytical undistortion formula, the disadvantage has not been emphasized since people tend to think that this problem can be solvable by the three methods listed at the beginning of Sec. 2.1. The main purpose of this work is to study alternative distortion functions, either polynomials or simple functions of the polynomials, with least amount of model complexity and as few distortion coefficients as possible, to achieve a comparable (or even better) calibration accuracy compared with the most commonly used radial distortion model (6), with an additional appealing property of having analytical closed-form inverse formula. As shown in Sec. 4, this additional appealing property might be achieved at the cost of adding one extra distortion coefficient.

(b) **How to extend to include tangential distortion?** Though this paper is mainly focused on the radial distortion modelling, it is worthy pointing out that the class of rational functions can also be applied to model geometric lens distortions by:

$$x_d = x\, f(r, \mathbf{k}_1), \quad y_d = y\, f(r, \mathbf{k}_2), \qquad (26)$$

where $f(r, \mathbf{k})$ can be any function in Table 2. Notice that when $\mathbf{k}_1 = \mathbf{k}_2$, the above equation reduces to the radial distortion modelling. The geometric distortion modelling in (26) allows the use of two different sets of distortion coefficients to model the distortions along the two image axes. Equation (26) denotes a lumped distortion model that aims to include all the nonlinear distortion effects.

6. Concluding Remarks

This paper proposes a new class of rational radial distortion models. The appealing part of these distortion models is that they preserve high accuracy together with easy analytical undistortion formulae. Performance comparisons are made between this class of new rational models and the existing polynomial models, based on an initial observation of the fit-

ting residue, the GAIC and GMDL criteria, and evaluation of the distortion only. Experiments results are presented to show that this new class of rational distortion models can be quite accurate and efficient, especially when the actual distortion is significant.

Acknowledgments

The authors would like to thank the reviewers for their comments on adding more experiments to validate the proposed rational distortion functions.

References

Basu, A. and Licardie, S. (1995). Alternative models for fish-eye lenses. *Pattern Recognition Letters*, 16(4):433–441.

Brauer-Burchardt, C. and Voss, K. (2001). A new algorithm to correct fish-eye- and strong wide-angle-lens-distortion from single images. In *Int. Conf. on Image Processing*, pages 225–228.

Devernay, F. and Faugeras, O. (2001). Straight lines have to be straight. *Machine Vision and Applications*, 13(1):14–24.

El-Melegy, M. T. and Farag, A. A. (2003). Nonmetric lens distortion calibration: Closed-form solutions, robust estimation and model selection. *IEEE Int. Conf. on Computer Vision*.

Fitzgibbon, A. W. (2001). Simultaneous linear estimation of multiple view geometry and lens distortion. In *Proceedings of the Conference on Computer Vision and Pattern Recognition*, pages 125–132, Kauai, Hawaii.

Hartley, R. and Zisserman, A. (2000). *Multiple View Geometry*. Cambridge University Press.

Heikkil, J. and Silvn, O. (1997). A four-step camera calibration procedure with implicit image correction. In *IEEE Computer Society Conference on Computer Vision and Pattern Recognition*, pages 1106–1112, San Juan, Puerto Rico.

Heikkila, J. (2000). Geometric camera calibration using circular control points. *IEEE Trans. on Pattern Analysis and Machine Intelligence*, 22(10):1066–1077.

Heikkila, J. and Silven, O. (1996). Calibration procedure for short focal length off-the-shelf CCD cameras. In *Proceedings of 13th Int. Conf. on Pattern Recognition*, pages 166–170, Vienna, Austria.

Kanatani, K. (2002). Model selection for geometric inference. In *The 5th Asian Conference on Computer Vision*.

Lenz, R. K. and Tsai, R. Y. (1988). Techniques for calibration of the scale factor and image center for high accuracy 3-D machine vision metrology. *IEEE Trans. on Pattern Analysis and Machine Intelligence*, 10(5):713–720.

Ma, L., Chen, Y., and Moore, K. L. (2003). Flexible camera calibration using a new analytical radial undistortion formula with application to mobile robot localization. In *IEEE International Symposium on Intelligent Control*, Houston, USA.

Ma, L., Chen, Y., and Moore, K. L. (May, 2002). Camera calibration: a USU implementation. CSOIS Technical Report, ECE Department, Utah State University, `http://arXiv.org/abs/cs.CV/0307072`.

Pearson, C. E., editor (1983). *Handbook of Applied Mathematics: Selected Results and Methods*. Van Nostrand Reinhold Company, second edition.

Slama, C. C., editor (1980). *Manual of Photogrammetry*. American Society of Photogrammetry, fourth edition.

Tamaki, T., Yamamura, T., and Ohnishi, N. (2002). Unified approach to image distortion. In *Int. Conf. on Pattern Recognition*, pages 584–587.

Tordoff, B. (2002). *Active Control of Zoom for Computer Vision*. PhD thesis, University of Oxford, Robotics Research Group, Department of Engineering Science.

Tsai, R. Y. (1987). A versatile camera calibration technique for high-accuracy 3D machine vision metrology using off-the-shelf TV cameras and lenses. *IEEE Journal of Robotics and Automation*, 3(4):323–344.

Wei, G. and Ma, S. (1994). Implicit and explicit camera calibration: theory and experiments. *IEEE Trans. on Pattern Analysis and Machine Intelligence*, 16(5):469–480.

Weng, J., Cohen, P., and Herniou, M. (1992). Camera calibration with distortion models and accuracy evaluation. *IEEE Trans. on Pattern Analysis and Machine Intelligence*, 14(10):965–980.

Zhang, Z. (1996). On the epipolar geometry between two images with lens distortion. In *Int. Conf. on Pattern Recognition*, pages 407–411, Vienna.

Zhang, Z. (1998). Microsoft research technical report. `http://rese-arch.microsoft.com/~zhang/calib/`.

Zhang, Z. (1999). Flexible camera calibration by viewing a plane from unknown orientation. *IEEE Int. Conf. on Computer Vision*, pages 666–673.